STATISTICS OF THE TURBULENT/NON-TURBULENT INTERFACE IN A SPATIALLY EVOLVING MIXING LAYER

Antonio Attili
Clean Combustion Research Center
King Abdullah University of Science and Technology
Kingdom of Saudi Arabia
antonio.attili@kaust.edu.sa

Juan C. Cristancho
Clean Combustion Research Center
King Abdullah University of Science and Technology
Kingdom of Saudi Arabia

Fabrizio Bisetti
Clean Combustion Research Center
King Abdullah University of Science and Technology
Kingdom of Saudi Arabia
fabrizio.bisetti@kaust.edu.sa

ABSTRACT

The thin interface separating the inner turbulent region from the outer irrotational fluid is analyzed in a direct numerical simulation of a spatially developing turbulent mixing layer. A vorticity threshold is defined to detect the interface separating the turbulent from the non-turbulent regions of the flow and to calculate statistics conditioned on the distance from this interface. The statistics of the position of the two interfaces in the mixing layer, i.e., on the low- and high-speed sides, are characterized by a Gaussian distribution and evolve in the streamwise direction coherently with the self-similar behavior of the flow. A strong vorticity jump is observed at the interfaces, in agreement with the results for other free shear flows, such as turbulent jets and wakes. Far from the interfaces, the conditional vorticity recovers the value observed for the classical turbulent statistics in the middle of the layer. The thickness of the interfaces are found to be of the order of the Taylor's microscale, similarly to other shear flows. Finally, the local velocity of the interfaces with respect to the flow is of the order of the Kolmogorov velocity, confirming that entrainment is governed by the dynamics of the smallest scales.

INTRODUCTION

In shear flows, such as jets, wakes, and mixing layers, the turbulent and irrotational regions are separated by sharp interfaces (Corrsin & Kistler, 1955). The study of these interfaces has recently gained new attention (Hunt *et al.*, 2011). These layers play a crucial role in the development of the turbulent field and are important in turbulent combustion and cloud physics as they affect entrainment and mixing. Recent results include new insight on the entrainment process, which is dominated by the spreading of small scale vortices (Mathew & Basu, 2002; Westerweel *et al.*, 2005; Holzner & Lüthi, 2011), and on the characteristic thickness of the interface. The thickness is of the order of the Kolmogorov's scale in shear-free turbulence (Holzner & Lüthi, 2011) and Taylor's microscale in flows with mean shear (da Silva & Pereira, 2008; da Silva & Taveira, 2010).

Both numerical and experimental studies have addressed shear-free turbulence (Holzner *et al.*, 2008; Holzner & Lüthi, 2011), jets (Mathew & Basu, 2002; da Silva & Pereira, 2008; da Silva & Taveira, 2010; Westerweel *et al.*, 2005, 2009; Wolf *et al.*, 2012; Taveira & da Silva, 2013), and wakes (Bisset *et al.*, 2002), but no statistics conditioned on the distance from the interface have been reported for the mixing layer.

PRELIMINARIES

The direct numerical simulation (DNS) presented in this work is performed by solving the unsteady, incompressible Navier-Stokes equations. The parallel flow solver "NGA" (Desjardins *et al.*, 2008), developed at Stanford University, is used to solve the transport equations. The solver implements a finite difference method on a spatially and temporally staggered grid with the semi-implicit fractional-step method of Kim & Moin (1985). Velocity and scalar spatial derivatives are discretized with a second-order finite differences centered scheme.

A complete description of the flow parameters and methods used for the computation is provided in Attili & Bisetti (2012), together with a detailed analysis of the spatial evolution of the flow and velocity statistics in the transitional and fully developed turbulent regions. There-

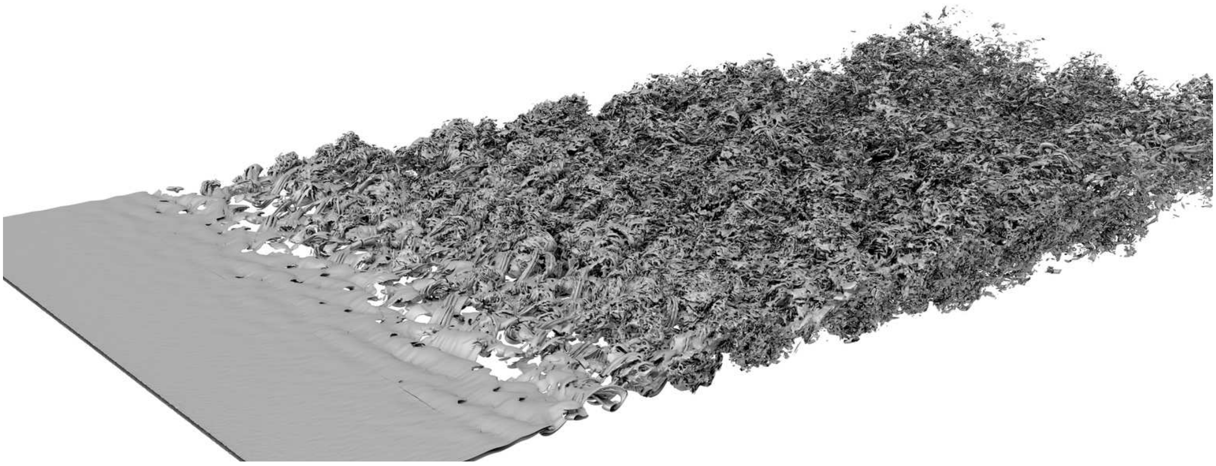

Figure 1. Isosurface of the vorticity magnitude. The whole domain is shown.

fore only a brief summary is presented here. The flow is imposed at the inlet plane ($x = 0$) and free convective outflow (Ol'Shanskii & Staroverov, 2000) is specified at $x = L_x$. The boundary conditions are periodic in the spanwise direction z and free-slip in the crosswise direction y. The flow at the inlet ($x = 0$) is a hyperbolic tangent profile for the streamwise velocity U with prescribed vorticity thickness $\delta_{\omega,0}$: $U(x=0,y,z) = U_c + 1/2\Delta U \tanh\left(2y/\delta_{\omega,0}\right)$, where $U_c = (U_1 + U_2)/2$ is the convective velocity, U_1 and U_2 are the high- and low-speed stream velocities and $\Delta U = U_1 - U_2$ is the velocity difference across the layer. The Reynolds number based on the vorticity (momentum) thickness at the inlet is $\mathrm{Re}_\omega = 600$ (resp. $\mathrm{Re}_\theta = 150$), increasing up to $\mathrm{Re}_\omega = 25,000$ (resp. $\mathrm{Re}_\theta = 4250$) as the mixing layer develops. The ratio of the two velocities is $U_1/U_2 = 3$. Low amplitude white noise is superimposed on the hyperbolic tangent profile, resulting in the onset of the Kelvin-Helmholtz instability at a short distance downstream of the inlet ($x \approx 50\delta_{\omega,0}$). The crosswise and spanwise velocity components are perturbed with the same type of disturbance.

The computational domain extends over $L_x = 473\delta_{\omega,0}$, $L_y = 290\delta_{\omega,0}$, $L_z = 157.5\delta_{\omega,0}$ in the streamwise (x), crosswise (y) and spanwise (z) directions, respectively. The domain is discretized with $3072 \times 940 \times 1024 \approx 3 \times 10^9$ grid points ($N_x \times N_y \times N_z$). In the region centered around $y = 0$ ($|y| \leq 45\delta_{\omega,0}$), the grid is homogeneous in the three directions: $\Delta x = \Delta y = \Delta z = 0.15\delta_{\omega,0}$. Outside the core region for $|y| > 45\delta_{\omega,0}$, the grid is stretched linearly until $\Delta y = 0.6\delta_{\omega,0}$ at $|y| = 55\delta_{\omega,0}$ and then is constant again up to the boundary. Overall, the spatial resolution is such that $\Delta x = \Delta y = \Delta z \leq 2.5\eta$ everywhere, where $\eta = \nu^{3/4}\varepsilon^{-1/4}$ is the Kolmogorov scale and ε the average turbulent kinetic energy dissipation. The time step size is calculated in order to have a unity Courant-Friedrichs-Lewy (CFL) number.

The simulation was performed on the IBM Blue Gene/P system "Shaheen" available at King Abdullah University of Science and Technology, using up to 65,536 processing cores (16 racks of the Blue Gene/P architecture). Statistics were accumulated over time for 3500τ ($\tau = \Delta U/\delta_{\omega,0}$) and 1400 flow field samples were used to evaluate statistics. Several time signals were sampled at various spatial locations to complement the spatial statistics with their temporal surrogates by Taylor's hypothesis.

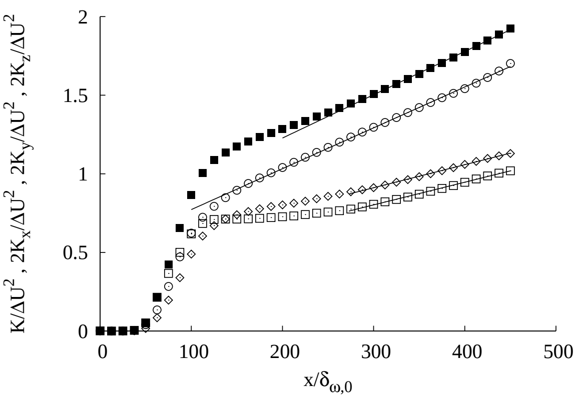

Figure 2. Streamwise evolution of normalized total turbulent kinetic energy $K/\Delta U^2$ (solid squares). Contributions from the three components of velocity are also shown: $2K_x/\Delta U^2$ (open circles), $2K_y/\Delta U^2$ (open squares), and $2K_z/\Delta U^2$ (open diamonds). Lines indicate least-square fit over $200 < x/\delta_{\omega,0} < 400$ (K_x) and $300 < x/\delta_{\omega,0} < 400$ (K, K_y and K_z).

The simulation required around 10 million CPU hours and produced approximately 100 TB of data.

Figure 1 shows an isosurface of the vorticity magnitude for the entire domain, highlighting the large scale vortices due to the Kelvin-Helmholtz instability and the small scale structures in the far field.

It is well known that at a certain distance from the inlet, the mixing layer evolves self-similarly. Appropriate scaling velocity and length scales are the constant velocity difference ΔU across the mixing layer and a measure of the local layer thickness, e.g. momentum or vorticity thickness (Pope, 2000). Self-similarity implies a linear growth for the total turbulent kinetic energy (Clark & Zhou, 2003): $K(x) = \int k dy = 1/2 \int \left(\langle uu \rangle + \langle vv \rangle + \langle ww \rangle\right) dy$, where $\langle\rangle$ is a statistical mean obtained by averaging in the spanwise direction z and time t and $u = U - \langle U \rangle$, $v = V - \langle V \rangle$, and $w = W - \langle W \rangle$ are the velocity fluctuations in the three directions. Figure 2 shows that the self-similar behavior (linear growth of turbulent kinetic energy and of its compo-

Table 1. Flow parameters in the far field of the mixing layer. The values of the Kolmogorov scale, production and dissipation are calculated at the crosswise position of maximum turbulent kinetic energy ($y \approx -5\delta_{\omega,0}$). $L_s = \sqrt{\varepsilon/\mathscr{S}^3}$ is the shear length scale, $\mathscr{S}$ being the local mean shear and ε the dissipation.

Kolmogorov scale	η	$0.07\delta_{\omega,0}$
Production/dissipation ratio	P/ε	1.4
Resolution	$\Delta x/\eta$	2
Shear length scale	L_s	$\approx 40\eta$
Vorticity thickness	δ_ω	$\approx 500\eta$
Taylor microscale	λ	$\approx 43\eta$
Reynolds number	Re_λ	≈ 250

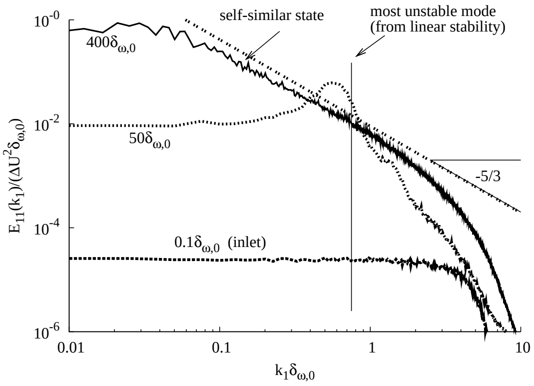

Figure 3. Spectra of streamwise velocity in the streamwise direction (L_{11}) at several downstream locations.

nents) is recovered for $x > 300\delta_{\omega,0}$, after a transition region dominated by the Kelvin-Helmholtz instability. The contribution of the streamwise component to the total kinetic energy (K_x) achieves self-similarity before the two other components (K_y and K_z). In the region where strong vortex pairing occurs, the crosswise component (K_y) of the turbulent kinetic energy undergoes rapid growth (Rogers & Moser, 1994; Attili & Bisetti, 2012) resulting in $K_y \geq K_x$ for $50\delta_{\omega,0} < x < 100\delta_{\omega,0}$.

Figure 3 shows the streamwise evolution of the L_{11} spectra in the center of the layer, at several streamwise locations. Downstream of the onset of the Kelvin-Helmholtz instability the flow becomes fully turbulent with spectra characterized by Kolmogorov's scaling over more than one decade in wavenumber space. Table 1 summarizes some important flow parameters in the far field of the mixing layer.

RESULTS

The interface between the turbulent and non-turbulent region is defined using a threshold on the value of the vorticity magnitude. The threshold value is around 30% of the mean vorticity in the core of the layer. Figure 4 shows the vorticity magnitude field in the streamwise/crosswise plane and the two interfaces between the core of the layer and the low- and high-speed irrotational regions (bottom and top, respectively). Both interfaces are highly convoluted and are

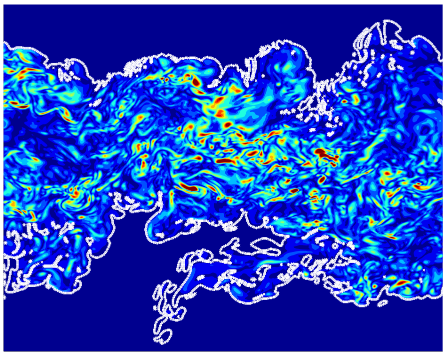

Figure 4. Vorticity magnitude in the self similar region. The threshold used to define the interface is also shown (white lines). The flow is from left to right and the low- (resp. high-) speed stream is on the bottom (resp. top).

characterized by a wide range of length scales. It is worth noting that the two interfaces appear different from a morphological perspective.

Following Mathew & Basu (2002), da Silva & Pereira (2008), and Westerweel *et al.* (2009), the interface *envelope* has been defined using the outermost points of the interface along lines at a given streamwise location. A statistical analysis of the position of the interface in the crosswise direction is shown in Figure 5. As expected, the position of the bottom (top) interface shifts downward (upward) moving downstream. From the histogram of the interface position, it is evident that both interfaces penetrate deep into the layer, reaching its center. However, the probability of this happening is rather low. The probability density functions (PDF) of the position of both the interfaces are very close to Gaussian distributions. This is in agreement with the measurements by Westerweel *et al.* (2009) for a turbulent round jet. The mean position of the interfaces is characterized by a linear evolution in the streamwise direction, consistently with the self-similarity assumption for the mixing layer. Also the variance of the position of the interfaces increases linearly in the streamwise direction.

Turbulence statistics are computed conditioned on the distance from the envelope and compared with classical statistics obtained averaging in time and statistical homogeneous directions (the spanwise direction in the present case). As suggested by da Silva & Pereira (2008), patches of engulfed irrotational fluid are removed from the conditional statistics. Figure 6 shows the statistics of the spanwise component of vorticity, both in the form of classical turbulence statistics and conditioned on the distance from the two interfaces. If rescaled with the local thickness of the layer and the velocity difference between the two streams, the profiles show self-similarity, with the exception of the first streamwise position located in the transitional region. For the conditional profiles, the distance from the interface is rescaled with the local Taylor's microscale, as suggested by da Silva & Pereira (2008). Moving from the non-turbulent region towards the core of the layer, the conditional mean profiles show a jump at both interfaces, reach a peak at a very short distance from the interface and then converge to a constant value close to the peak of the classical mean profiles in the middle of the layer. While the non-dimensional

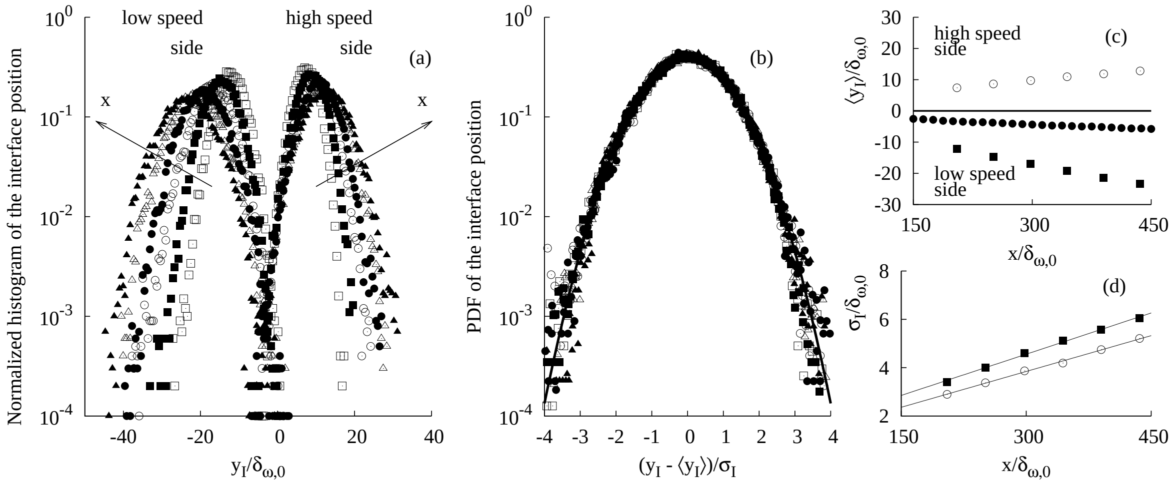

Figure 5. Statistics of the crosswise position of the two interfaces. (a): Histograms of the position at different streamwise locations: $x/\delta_{\omega,0} = 205$ (open squares), $x/\delta_{\omega,0} = 251$ (filled squares), $x/\delta_{\omega,0} = 298$ (open circles), $x/\delta_{\omega,0} = 344$ (filled circles), $x/\delta_{\omega,0} = 390$ (open triangles), $x/\delta_{\omega,0} = 436$ (filled triangles). (b): Probability density functions of the interfaces position, normalized with the first two moments. The solid line is a normal distribution (Gaussian) with zero mean and unity variance. (c): Streamwise evolution of the mean position of the interface for the high- (open circles) and low-speed side (filled squares). The filled circles indicate the center of the layer, moving towards the low-speed stream. (d): Streamwise evolution of the variance of the interface position for the high- (open circles) and low-speed side (filled squares).

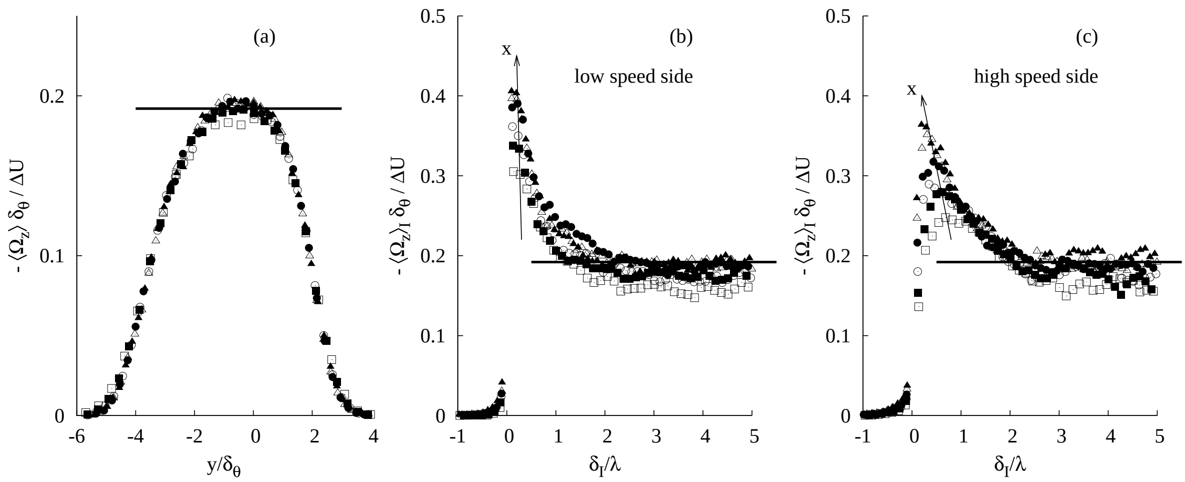

Figure 6. Vorticity statistics. (a): Crosswise profiles of the mean of the spanwise component of vorticity. The local momentum thickness of the layer δ_θ and the velocity difference between the two streams ΔU are used for non-dimensionalization. (b-c): Mean spanwise vorticity conditioned on the distance from the interface for the low- and high-speed sides of the layer. The distance from the interface δ_I is scaled with the Taylor's microscale in the center of the layer. Different symbols for different streamwise positions: $x/\delta_{\omega,0} = 205$ (open squares), $x/\delta_{\omega,0} = 251$ (filled squares), $x/\delta_{\omega,0} = 298$ (open circles), $x/\delta_{\omega,0} = 344$ (filled circles), $x/\delta_{\omega,0} = 390$ (open triangles), $x/\delta_{\omega,0} = 436$ (filled triangles). The solid horizontal line in (a) indicates the maximum of the mean and is shown also in (b) and (c) for comparison.

value of mean vorticity far from the interface reaches a self-similar behavior, the peak continues to increase moving in the streamwise direction. From the present calculation it is unclear whether this is a residual of the transition or a genuine characteristic of the turbulence in the fully developed region. It is apparent that rescaling the distance from the interface with the Taylor's microscale λ generates a good collapse of all the profiles, confirming the observation made in other shear flows that the thickness of the interface scale with λ (da Silva & Pereira, 2008; da Silva & Taveira, 2010).

Statistics of vorticity conditioned on the distance from the interfaces have been reported for a number of different shear flows (Mathew & Basu, 2002; da Silva & Pereira, 2008; da Silva & Taveira, 2010; Westerweel *et al.*, 2005, 2009; Wolf *et al.*, 2012; Taveira & da Silva, 2013; Bisset *et al.*, 2002), so it is of interest to compare the results for the mixing layer with those obtained in other configurations. Figure 7 shows the conditional profiles of the enstrophy (i.e., the vorticity magnitude) for the mixing layer and other shear flows. The similar behavior for the different flows suggests a degree of universality in the vorticity dynamics near the turbulent non-turbulent interface.

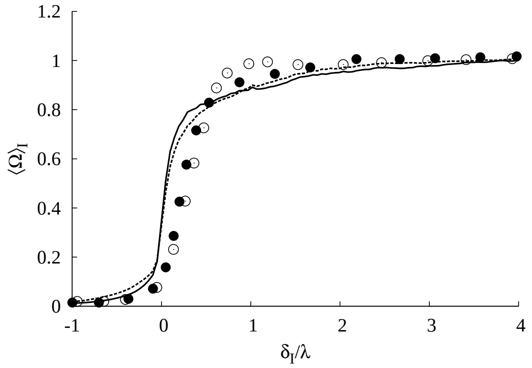

Figure 7. Conditional average of the vorticity magnitude for the low- (solid line) and high-speed stream (dashed line) compared with the results by da Silva & Taveira (2010) for a round jet (filled symbols) and by Bisset *et al.* (2002) for a wake (open symbols). The profiles are scaled with the Taylor's microscale and the value of the vorticity magnitude far from the interface.

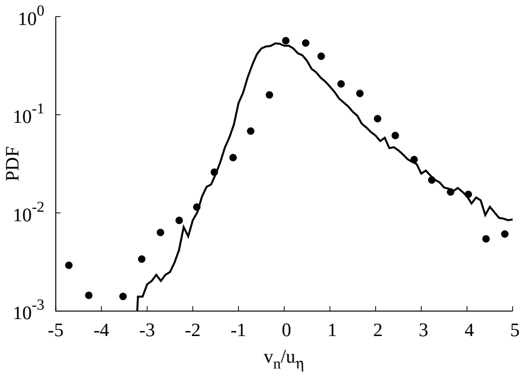

Figure 8. Probability density function of the interface velocity (eq. 1) in the mixing layer (line) compared with the results by Holzner & Lüthi (2011) for sheer-free turbulence (symbols).

Holzner & Lüthi (2011) analyzed the velocity, relative to the fluid, of the interfaces separating the turbulent and non-turbulent regions in flows without mean shear. The relative velocity is defined as (Holzner & Lüthi, 2011):

$$v_n = -\frac{2\omega_i\omega_j s_{ij}}{|\nabla\omega^2|} - \frac{2\nu\nabla^2\omega_i}{|\nabla\omega^2|}, \qquad (1)$$

where ω_i is the vorticity vector, s_{ij} the rate of strain tensor, and ν the kinematic viscosity. Figure 8 shows the probability density function (PDF) of v_n for the top interface. The interface velocity v_n is normalized with the mean Kolmogorov velocity u_η, calculated at the interface. The mean and standard deviation are close to u_η and the overall PDF is in good agreement with the result by Holzner & Lüthi (2011) notwithstanding the differences in the two configurations, i.e. mixing layer versus shear-free turbulence. These observations confirm that that the appropriate scales describing the spreading of the interface are the Kolmogorov's length and velocity, suggesting that, even if the interface thickness scales with the Taylor's scales, entrainment is governed by the dynamics of the smallest scales.

REFERENCES

Attili, A. & Bisetti, F. 2012 Statistics and scaling of turbulence in a spatially developing mixing layer at $\mathrm{Re}_\lambda = \mathbf{250}$. *Phys. Fluids* **24** (3), 035109.

Bisset, D.K., Hunt, J.C.R. & Rogers, M.M. 2002 The turbulent/non-turbulent interface bounding a far wake. *J. Fluid Mech.* **451**, 383–410.

Clark, T.T. & Zhou, Y. 2003 Self-similarity of two flows induced by instabilities. *Phys. Rev. E* **68** (6), 66305.

Corrsin, S. & Kistler, A.L. 1955 Free-stream boundaries of turbulent flows. *Tech. Rep.* TN-1244. NACA, Washington, DC.

Desjardins, O., Blanquart, G., Balarac, G. & Pitsch, H. 2008 High order conservative finite difference scheme for variable density low Mach number turbulent flows. *J. Comput. Phys.* **227** (15), 7125–7159.

Holzner, M., Liberzon, A., Nikitin, N., Lüthi, B., Kinzelbach, W. & Tsinober, A. 2008 A lagrangian investigation of the small-scale features of turbulent entrainment through particle tracking and direct numerical simulation. *J. Fluid Mech.* **598**, 465.

Holzner, M. & Lüthi, B. 2011 Laminar superlayer at the turbulence boundary. *Phys. Rev. Lett.* **106** (13), 134503.

Hunt, J.C.R., Eames, I., da Silva, C.B. & Westerweel, J. 2011 Interfaces and inhomogeneous turbulence **369** (1937), 811–832.

Kim, J. & Moin, P. 1985 Application of a fractional-step method to incompressible Navier-Stokes equations. *J. Comput. Phys.* **59** (2), 308–323.

Mathew, J. & Basu, A.J. 2002 Some characteristics of entrainment at a cylindrical turbulence boundary. *Phys. Fluids* **14**, 2065.

Ol'Shanskii, M.A. & Staroverov, V.M. 2000 On simulation of outflow boundary conditions in finite difference calculations for incompressible fluid. *Int. J. Numer. Methods Fluid* **33** (4), 499–534.

Pope, S.B. 2000 *Turbulent flows*. Cambridge Univ Pr.

Rogers, M. M. & Moser, R. D. 1994 Direct simulation of a self-similar turbulent mixing layer. *Phys. Fluids* **6**, 903.

da Silva, C.B. & Pereira, J.C.F. 2008 Invariants of the velocity-gradient, rate-of-strain, and rate-of-rotation tensors across the turbulent/nonturbulent interface in jets. *Phys. Fluids* **20**, 055101.

da Silva, C.B. & Taveira, R.R. 2010 The thickness of the turbulent/nonturbulent interface is equal to the radius of the large vorticity structures near the edge of the shear layer. *Phys. Fluids* **22**, 121702.

Taveira, R.R. & da Silva, C.B. 2013 Kinetic energy budgets near the turbulent/nonturbulent interface in jets. *Phys. Fluids* **25**, 015114.

Westerweel, J., Fukushima, C., Pedersen, J.M. & Hunt, J.C.R. 2005 Mechanics of the turbulent-nonturbulent interface of a jet. *Phys. Rev. Lett.* **95** (17), 174501.

Westerweel, J., Fukushima, C., Pedersen, J.M. & Hunt, J.C.R. 2009 Momentum and scalar transport at the turbulent/non-turbulent interface of a jet. *J. Fluid Mech.* **631**, 199.

Wolf, M., Lüthi, B., Holzner, M., Krug, D., Kinzelbach, W. & Tsinober, A. 2012 Investigations on the local entrainment velocity in a turbulent jet. *Phys. Fluids* **24**, 105110.